ESASGD 2016

ISBN: 978-604-76-1171-3

NOT FOR SALE

INTERNATIONAL CONFERENCES ON EARTH SCIENCES AND SUSTAINABLE GEO-RESOURCES DEVELOPMENT

Hanoi University of Mining and Geology

Proceedings of the ESASGD 2016

Hanoi, November 12-15, 2016

Session: Geoinformatics for Natural Resources, Hazards and Sustainability (GIS IDEAS 2016)

ISBN:978-604-76-1171-3

TRANSPORT PUBLISHING HOUSE

TABLE OF CONTENTS

Available online at *gisws.media.osaka-cu.ac.jp/gisideas16/*

ESASGD 2016

GIS-IDEAS 2016

International Conference on GeoInformatics for Spatial-Infrastructure Development in Earth & Allied Sciences (GIS-IDEAS)

A Quantitative Assessment of Algorithm for Increasing Gridded DEM resolution using the Hopfield Neural Network

Nguyen Quang MINH[a*], Pham Thanh THAO[a], Nguyen Thi Thu HUONG[a], La phu HIEN[a], H.G. Lewis[b], P.M. Atkinson[c, d, e]

[a] *Faculty of Geomatics and Land Administration, Hanoi University of Mining and Geology, nguyenquangminh@humg.edu.vn*
[b]*Astronautics Research Group, University of Southampton, Highfield, Southampton SO17 1BJ, UK*
[c] *Faculty of Science and Technology, Engineering Building, Lancaster University, Lancaster LA1 4YR*
[d] *School of Geography, Archaeology and Palaeoecology, Queen's University Belfast, BT7 1NN, Northern Ireland, UK*
[e] *Geography and Environment, University of Southampton, Highfield, Southampton SO17 1BJ, UK*

Abstract

A model for increasing the spatial resolution of a digital elevation model in grid form (Gridded DEM) is proposed. The downscaling model works by minimising the local semivariance as a goal, and by matching the original coarse spatial resolution elevation value as a constraint. The approach was coded into a simple Hopfield neural network (HNN) model in which each pixel of the original coarse DEM is divided into m×m sub-pixels. The elevation of each sub-pixel is derived iteratively (i.e. optimised) based on minimising the local semivariance and the elevation constraint. The activation function used in this model of HNN is a simple linear function. The proposed model was tested via an experiment using a Gridded DEM at 20 m, 60 m and 90 m resolutions. The assessment showed very promising results for increasing the spatial resolution of the Gridded DEM.

Keywords: Hopfield neural network, Grid DEM resolution enhancement, smoothing

1. Introduction

The spatial resolution of a Gridded DEM affects both the information content and the accuracy of the data and many other secondary data products (Saksena & Merwade, 2015). Examples include the well-known effects of DEM spatial resolution on the spatial properties of spatial data (Bian & Butler, 1999), and more specifically on slope and aspect (Chang & Tsai, 1991), watershed boundary delineation and the accuracy of SWAT schemes (Rawat, et al. 2014), water run-off models (Vieux 1993), three dimensional modelling of landscapes (Schoorl, Sonneveld and Veldkamp 2000), and soil survey results (Smith, et al. 2006). All of the above-mentioned research showed that DEMs with a finer spatial resolution can produce more informative and more accurate results.

Gridded DEMs with fine spatial resolution and high accuracy can be acquired using airborne Lidar technology or ground surveying or photogrammetry (Guo, et al. 2010). Airborne Lidar enables the acquisition of data with a very high density of 3 dimensional coordinate points and, therefore, it is possible to produce a DEM with sub-metre spatial resolution. However, airborne Lidar-derived DEMs have been used in many different applications, some of which require very fine spatial resolution and very high accuracy (Rapinel, et al. 2015).

* Corresponding author. Tel.: +84-043-838-7987.
E-mail address: nguyenquangminh@humg.edu.vn

Although possessing a great advantage in generating a fine spatial resolution DEM, airborne Lidar technology has some challenges such as the very large amount of data storage required and high computing capacity for data processing. Compared with airborne Lidar, other methods for fine spatial resolution DEM acquisition such as ground surveying and photogrammetry are time consuming and labour-intensive (Liu 2008).

The raster data can be downscaled using several resampling approaches. The most used approaches for downscaling are bilinear and bi-cubic interpolation. Other methods can also be used such as B-spline resampling and the filtering method used in a patent by Atkins, et al., 2000. The downscaling for raster data can somehow increase the spatial resolution of these data and the produced data can be used in a Gridded DEM.

Sub-pixel mapping is technique used to predict land cover at the sub-pixel scale using a soft-classified land cover proportions image as input (Atkinson 1997). In term of geographical scaling, sub-pixel mapping approaches are downscaling techniques which use the soft-classified land cover proportions as a constraint and maximise the spatial dependence between sub-pixels as tools to increase the spatial resolution (Su, et al., 2012). Several sub-pixel mapping techniques have been developed such as sub-pixel swapping, Markov random field, Hopfield neural network (HNN) (Tatem, et al. 2001; Nguyen, Atkinson and Lewis 2005). The HNN technique has been modified for smoothing and increasing the spatial resolution of raw multispectral remotely sensed imagery (Minh, 2011). Because both remote sensing images and Gridded DEMs are provided in the raster data model, it is expected that the approaches developed for remote sensing images may be applied to increase the Gridded DEM spatial resolution.

2. Method

2.1. HNN approach for sub-pixel mapping

The model for increasing the spatial resolution of a Gridded DEM increasing is a modified version of the Hopfield Neural Network HNN designed for super-resolution sub-pixel mapping (Tatem, et al., 2001 and Nguyen, et al., 2011). In the HNN for super-resolution sub-pixel mapping, an original pixel are is devided into m×m sub-pixels and each sub-pixel is represented by a neuron in the HNN. This particular model is based on an area proportions constraint and two goal functions. The proportion constraint is to ensure that the total number of sub-pixels of each land cover class must be equal to the number of sub-pixels assigned by the soft-classified land cover proportion. The goal functions play the role of a spatial dependence engine, which increases the tendency of adjacent sub-pixels to belong to the same land cover class.

In the HNN used for super-resolution sub-pixel mapping, the output vij of a neuron (sub-pixel) (i, j) is:

$$v_{ij} = g(u_{ij}) = 0.5\left(1 + \tanh(\lambda u_{ij})\right) \quad (1)$$

here $g(u_{ij})$ is an activation function of each neuron, u_{ij} is the input value of each neuron and λ is stepness value, which is defined empirically as 100.

The input value u_{ij} is determined at the time t as

$$u_{ij}(t) = u_{ij}(t-dt) + \frac{du_{ij}}{dt}dt \quad (2)$$

Where dt is time step, $v_{ij}(t-dt)$ is the output value at the time $(t-dt)$ and $\frac{du_{ij}}{dt}$ defined as follows:

$$\frac{du_{ij}}{dt} = -\frac{dE}{dv_{ij}} \quad (3)$$

where, E is energy, is defined as E = Goals + Constraint and

$$\frac{dE}{dv_{ij}} = \sum_{k}\frac{dG_k}{dv_{ij}} + \frac{dC}{dv_{ij}} \quad (4)$$

where, K is the number of Goal functions. Depending on the specific application, the goal and constraint functions can be modified for optimization. In Tatem et. al. (2001), the Goal functions are the two Goal functions for spatial dependence maximization, and the Constraint Functions comprise an Area Constraint function used for retaining the area proportions predicted by the soft-classification and a Multi-class Function which ensures that a sub-pixel belongs to only one class. In Nguyen et. al. (2011), a Panchromatic Constraint Function was added to the HNN model of Tatem et. al. to increase the accuracy of the sub-pixel mapping results.

The running of HNN in this the above cases is terminated when the total energy E of the HNN reaches a minimum value determined as

$$E = \sum Goals + \sum Constraint = min$$

Or:

$$E(t) - E(t-dt) = 0 \quad (5)$$

2.2. Proposed HNN approach for Grid DEM downscaling

The newly proposed approach is based on the assumption that the elevation of each sub-pixel must be close to its adjacent sub-pixels (spatial dependence assumption). The realization of spatial dependence in this case is calculated using the semivariance which can be defined as

$$\gamma(h) = \frac{1}{2N(h)}\sum_{1}^{N(h)}\left[v_{ij} - v_{ij+h}\right]^2 \tag{6}$$

where $\gamma(h)$ is the semivariance value at lag distance h, h is distance between a pair of data points v_{ij} and v_{ij+h}, and N(h) is the number of pairs of data points. If the points are spatially dependent, the semivariance will be small at small lag h. This means that the spatial dependence is largest when the semivariance is smallest (with small lag h), and minimizing the semivariance means maximizing the spatial dependence. The minimum value of semivariance can be defined based on the derivative as

$$\frac{\partial\gamma(h)}{\partial v} = 0 \tag{7}$$

and,

$$\frac{\partial\gamma(h)}{\partial v} = \frac{1}{2N(h)}\sum_{1}^{N(h)}\left(2v_{ij} - 2v_{ij+h}\right) = v_{ij} - \frac{\sum_{1}^{N(h)} v_{ij+h}}{N(h)} \tag{8}$$

So,

$$v_{ij}^{expected} = \frac{\sum_{1}^{N(h)} v_{ij+h}}{N(h)} \tag{9}$$

The change in elevation of each sub-pixel from the spatial dependence maximization operation is

$$du_{ij}^{sd} = v_{ij}^{expected} - v_{ij} \tag{10}$$

This means that the expected value of data points v_{ij} is the average of the values of all data points with lag h (v_{ij+h}). In this model for Gridded DEM, the data points with smallest lag h are the 8 pixels surounding the pixel v_{ij}. This function can be called as the spatial dependence maximization function.

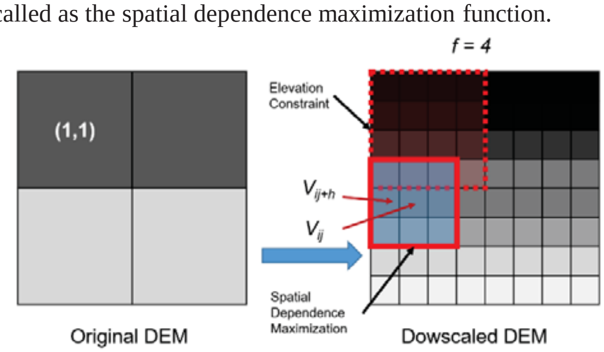

Fig. 1 Downscaling of Gridded DEM by a factor of 4

The newly proposed model developed for smoothing a Gridded DEM is presented in Figure 1 for the case of a DEM of size 2×2 pixels. A pixel in the original DEM is divided into 4×4 sub-pixels in the new DEM (zoom factor f = 4). So the original image of 2×2 pixels is resampled to an image of 8×8 sub-pixels. Each sub-pixel is represented by a neuron in the HNN model where the initial value is the elevation value of the pixel in the original DEM (or may be assigned randomly). An expected elevation of sub-pixel from the spatial dependence maximization function is calculated using a 3×3 window and the value of the central sub-pixel is equal to the average of the 8 surounding sub-pixels.

If the spatial dependence maximizing function is the only function used in the model, the elevation of all sub-pixels in the new DEM will be finally the same and the coarse elevation values of the original DEM will not be presered. To resolve this problem, a simple constraint function is used. The principle of this constraint is the average of elevation of all sub-pixels located within a pixel of original DEM must be equal to the elevation of the original pixel. For example, the average of the elevation of all sub-pixels within the area of the pixel (1,1) of the original image in **Error! Reference source not found.** must be equal to the elevation of the pixel (1,1).

$$du_{ij}^{ep} = Elevation_{x,y} - \frac{\sum_{(x-1)\times m}^{x\times m}\sum_{(y-1)\times m}^{y\times m} v_{pq}}{m\times m} \tag{11}$$

where $Elevation_{x,y}$ is the elevation value of the pixel (x, y) in the original image, v_{pq} is the sub-pixel (p, q) covered by pixel (x, y) in the newly generated image, and m is zoom factor. If the average of the elevation values of all sub-pixels within a pixel is smaller than the $Elevation_{x,y}$, then a value is added to the elevation value v_{pq} of all sub-pixels covered by pixel (x, y). In contrast, when the average of the elevation values of all sub-pixels within pixel (x, y) is larger than the $Elevation_{x,y}$, a value is substracted from the output value v_{pq} of the neuron (p, q).

Then an input value of each neuron (sub-pixel) can be calculated based on the Formula (2) with the value du_{ij}/dt is

$$\frac{du_{ij}}{dt} = \frac{dE_{ij}}{dv} = du_{ij}^{sd} + du_{ij}^{ep} \tag{12}$$

The output value v_{ij} of each neuron is then calculated using an activation function $g(u_{ij})$. However, in this new model, the activation function $g(u_{ij})$ is not like in Formula 1 because it is not used for pushing the output value of the neurons to 0 or 1 as in the case of sub-pixel mapping. Instead, a linear activation function presented in reasearch by Tank and Hopfield (Tank & Hopfield, 1986) was used in this new approach as

$$v_{ij} = g(u_{ij}) = a \times u_{ij} + b \tag{13}$$

where, parameters a = 1 and b = 0 in this model.

The HNN network runs until the energy is minimized as

$$E = \sum_i \sum_j \left(du_{ij}^{sd} + du_{ij}^{ep}\right) = min \tag{14}$$

or, the $E(t) - E(t - dt) = 0$, where (t - dt) and t are two consecutive iterations of the Hopfield Neural Network.

3. Quantitative assessment of the algorithm

3.1. Reference and testing data

There are three sets of DEM data at different spatial resolutions used for evaluating the algorithm. The first set of data were collected using ground surveying in Lang Son Province of Vietnam. The area of the test field is about 200 m × 200 m in Mai Pha Ward, Lang Son City which is about 150 km from Hanoi. The collected point data were used to generate the DEM data for use as a reference at 5 m spatial resolution, as can be seen in **Error! Reference source not found.**(a).

The second set of testing data were about 3.5 km × 3.5 km collected at Yen Thanh District, Nghe An Province, in the North Central of Vietnam. The location of the area is about 180 58' 57.03" N, 1050 22' 44.87" E, about 45 km from Vinh City. The resolution of original DEM is at 20 m (**Error! Reference source not found.**(a)) and this was downgraded into 60 m DEM for testing the algorithm (**Error! Reference source not found.**(b)). The third DEM data was also collected at the same area with the second DEM with the resolution of 30 m (**Error! Reference source not found.**(a)) and this is also downgraded to 90 m to make to input for the algorithm (**Error! Reference source not found.**(b)). This is SRTM DEM obtained from USGS Earth Explorer (http://earthexplorer.usgs.gov/).

3.2. Results and discussions

To test the proposed algorithm, a DEM with coarser resolution of 20 m was produced from the point elevation data as shown in **Error! Reference source not found.**(b). This 20 m spatial resolution DEM was then used as input for the proposed algorithm to produce a downscaled DEM at resolution of 5 m using bilinear, cubic smoothing and the proposed HNN downscaling algorithms (zoom factor of 4). The accuracy of this downscaled DEM was assessed based on comparison of the root mean squared error (RMSE) of resulted DEM from bilinear (**Error! Reference source not found.**(d)), cubic smoothing (**Error! Reference source not found.**(e)) and HNN downscaling algorithm (**Error! Reference source not found.**(c)). Similarly, the downgraded 60 m and 90 m DEM in Nghe An then were also used as inputs for the algorithms to produce the downscaled DEM at the resolution of 20 m and 30 m, respectively, using bilinear, cubic and proposed downscaling algorithms with the zoom factor of 3 (**Error! Reference source not found.** and **Error! Reference source not found.**).

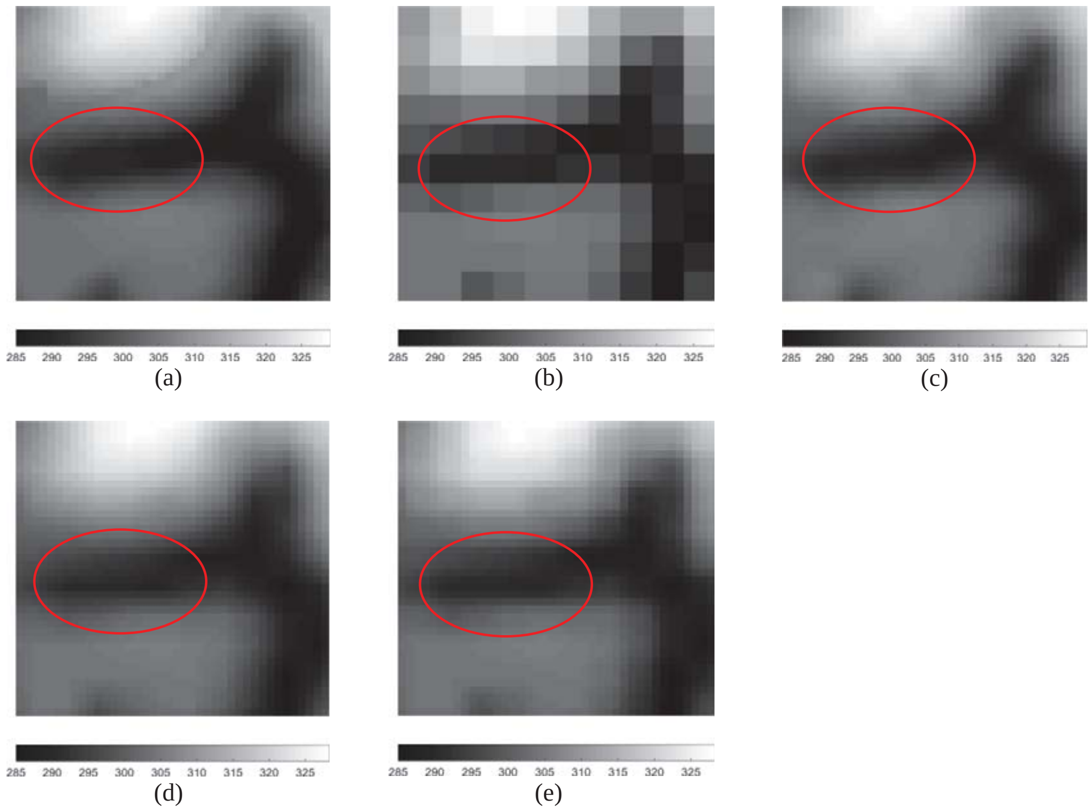

Fig. 2 Downscaling of DEM data. (a) Reference DEM data at 5 m resolution; (b) Downgraded DEM data at 20 m resolution; (c) downscaled DEM at 5 m resolution; (d) Bilinear smoothing DEM at 5 m resolution; and (e) Cubic smoothing DEM at 5 m resolution

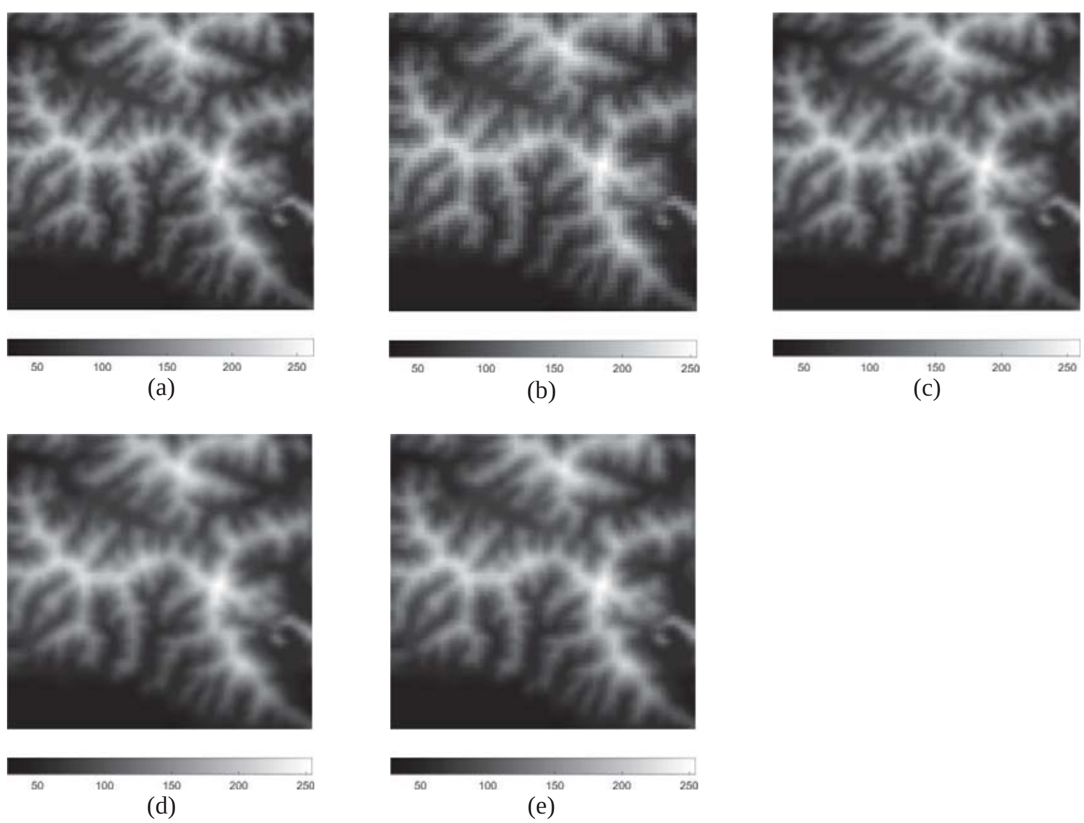

Fig. 3 Downscaling of DEM from 60 m to 20 m. (a) Reference DEM at 20 m resolution; (b) Downgraded DEM at 60 m resolution; (c) Downscaled DEM at 20 m resolution; (d) Bilinear smoothed DEM at 20 m; and (e) Cubic smoothed DEM at 20 m resolution.

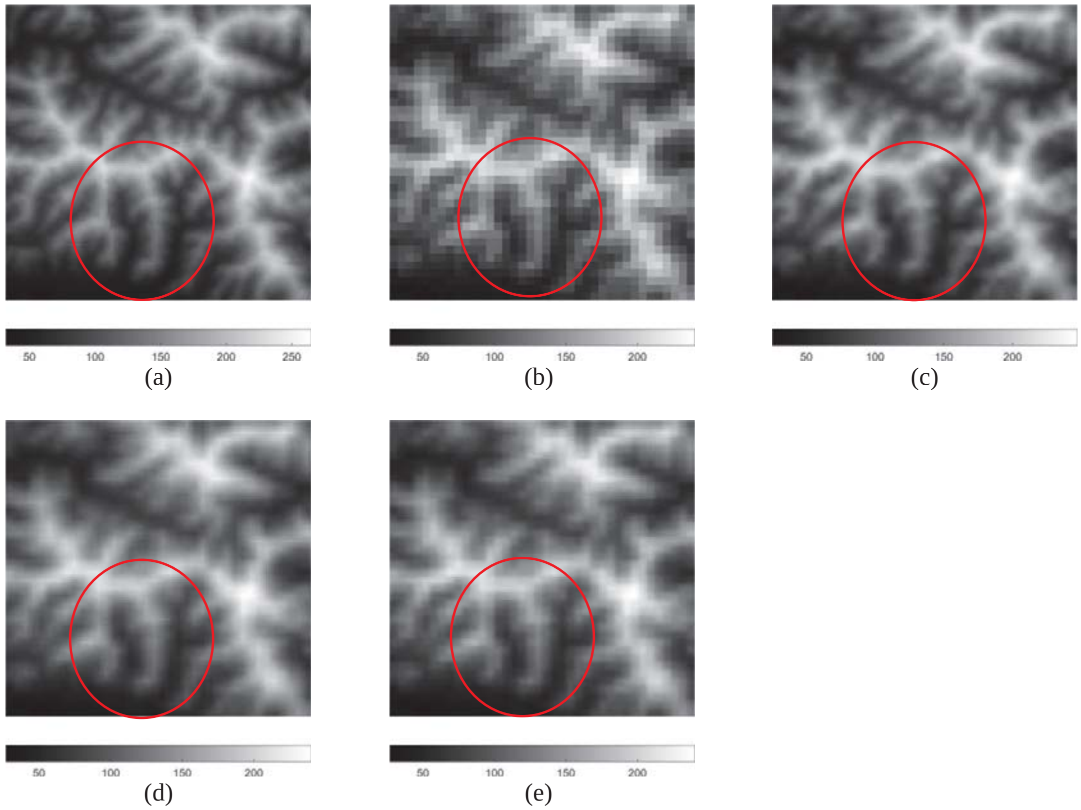

Fig. 4 Downscaling of DEM from 90 m resolution to 30 m resolution. (a) Reference DEM at 30 m resolution; (b) Downgraded DEM at 90 m resolution; (c) Downscaled DEM at 30 m resolution; (d) Bilinear smoothed DEM 30 m resolution; and (e) Cubic smoothed DEM 30 m resolution.

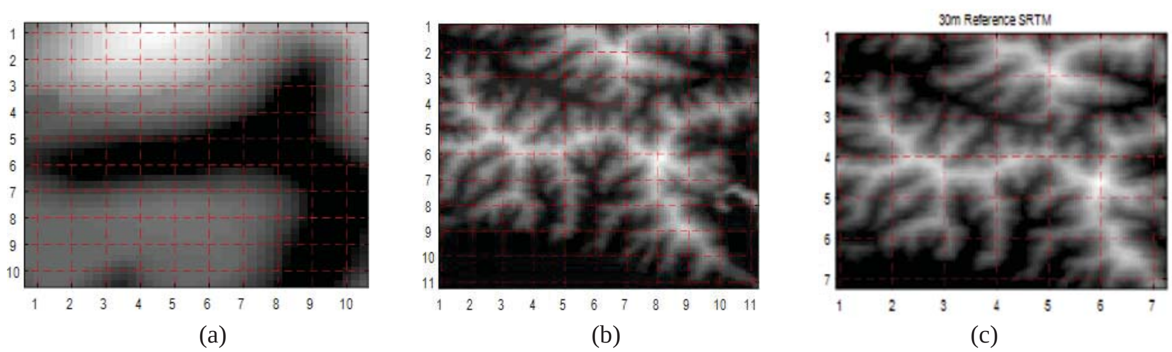

Fig. 5 Positions of the profiles for DEM; (a) 5 m DEM at Lang Son; 20 m DEM at Nghe An; and 30 m DEM at Nghe An

The assessment is implemented based on both visual comparisons of the resulted DEMs from different methods and the quantitative evaluation using RMSE (Table 1, Table 2, and Table 3). To evaluate the effects of the algorithms to different forms of the terrains, the cross-sections (profiles) were generated for visual comparison of the matching between the surface of the reference DEM, and coarse resolution surface, the surfaces generated by bilinear, cubic smoothing and HNN downscaling algorithm. The locations of the profiles for three data sets are presented as in Fig. 5(a), Fig. 5(b) and Fig. 5(c). Together with the visual comparison of the profiles, the RMSE of the profiles are also calculated for Lang Son data set, Nghe An 20 m resolution and 30 m resolution data sets, as in Table 1, Table 2 and Table 3, respectively.

The visual comparison showed that the resulted DEM from newly proposed HNN look more similar to the reference DEM than the coarse resolution and resulted DEMs from bilinear and cubic convolution methods. The improvement is clearly seen in comparison between the 5 m DEMs in Fig. 2(a) and Fig. 2(b), Fig. 2(c), Fig. 2(d) and Fig. 2(e). While the downscaled DEMs in Fig. 2(c) looks very similar to reference DEM in Fig. 2(a), the resulted DEMs from bilinear, and especially the cubic interpolation, were distorted due to the effects of the far away pixels to the central pixel.

Table 1 Root mean squared error for the results of smoothing and HNN downscaling algorithms with Lang Son 5 m DEM

Data sets	Original DEM (m)	Bilinear Smoothing (m)	Cubic Smoothing (m)	HNN downscaling (m)	Accuracy improvement (%)
Lang son 5 m DEM data	2.4571	1.5139	1.6000	0.8493	65.4
Column Cross section 1	1.4960	1.2419	1.2912	0.9734	34.9
Column Cross section 2	1.6962	1.1635	1.1821	0.5120	69.8
Column Cross section 3	2.0641	1.4043	1.4791	0.7383	64.2
Column Cross section 4	2.2345	1.3591	1.4586	0.7156	68.0
Column Cross section 5	2.2705	1.3006	1.3728	0.9587	57.8
Column Cross section 6	2.3084	1.7034	1.7805	0.8381	63.7
Column Cross section 7	2.0349	1.6198	1.6569	0.8068	60.4
Column Cross section 8	2.0325	1.4749	1.5564	0.8032	60.5
Column Cross section 9	2.0937	1.2861	1.3578	0.9988	52.3
Column Cross section 10	1.9876	1.2374	1.2959	0.9294	53.2
Row Cross section 1	1.9569	1.4024	1.4348	0.8798	55.0
Row Cross section 2	2.2873	1.6555	1.7196	0.7838	65.7
Row Cross section 3	2.3612	1.6712	1.7451	1.1155	52.8
Row Cross section 4	1.9510	1.4361	1.5174	0.5897	69.8
Row Cross section 5	1.7489	1.4228	1.4657	0.6816	61.0
Row Cross section 6	1.7289	1.4081	1.4297	1.1131	35.6
Row Cross section 7	1.6217	1.1567	1.2101	0.7876	51.4
Row Cross section 8	1.3897	0.8887	0.9730	0.6621	52.4
Row Cross section 9	1.4791	0.9317	0.9592	0.5098	65.5
Row Cross section 10	1.8042	1.4126	1.4593	0.6564	63.6

The difference between the HNN downscaled DEMs and DEMs created by smoothing methods is not clearly seen with two coarser data sets (20 m and 30 m) as with the 5 m DEM. However, the improvement is still visually shown in the area marked in Fig. 4 where a ridge was better reconstructed in the downscaled DEM image than in the bilinear and cubic smoothing DEM images.

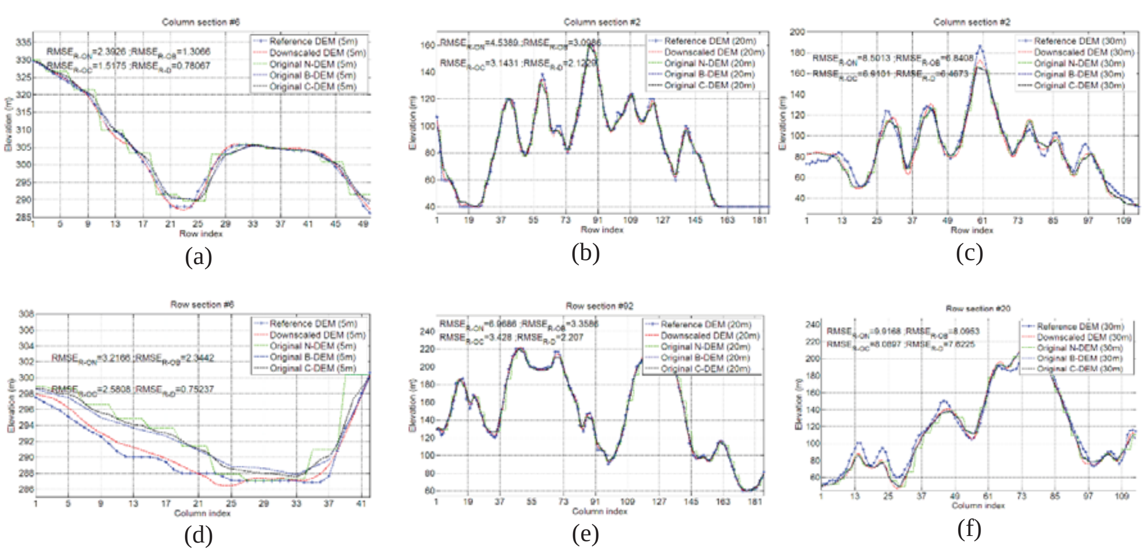

Fig. 6 Comparison of reference surface, HNN downscaled surface, original surface, bilinear interpolated surface and cubic surface based on profiles: (a) a column profile for 5 m data set, (b) a column profile for 20 m data set, (c) a column profile for 30 m data set, (d) a row profile for 5 m data set, (e) a row profile for 20 m data set, and (f) a row profile for 30 m data set,

The matching of surfaces represented by DEMs from different methods also showed an advantage of the HNN downscaling to the original coarse DEM and other smoothing methods. The profiles of HNN downscaled DEM matches very well with the profiles of the reference DEM while other methods' DEMs does not and this is most clearly seen with 5 m Lang Son data (Fig. 6(a) and Fig. 6(d)). In Fig. 6(d) of Row 6 profile, the surfaces

Table 2 Root mean squared error for the results of smoothing and HNN downscaling algorithms with Nghe An 20 m DEM

Data sets	Original DEM (m)	Bilinear Smoothing (m)	Cubic Smoothing (m)	HNN downscaling (m)	Accuracy improvement (%)
Nghe An 20 m DEM data	6.9326	3.3026	3.3716	1.9853	71.4
Column Cross section 1	4.5389	3.0986	3.1431	2.1229	53.2
Column Cross section 2	4.4169	2.8131	2.8973	1.7895	59.5
Column Cross section 3	4.3370	2.7674	2.8041	1.8675	56.9
Column Cross section 4	4.4689	2.9057	2.9731	2.0949	53.1
Column Cross section 5	4.0911	2.9148	2.9445	2.0043	51.0
Column Cross section 6	3.8029	2.5245	2.5619	1.9124	49.7
Column Cross section 7	4.6677	3.1959	3.2344	2.2049	52.8
Column Cross section 8	4.8884	2.9958	3.0833	2.0910	57.2
Column Cross section 9	5.1846	2.9851	3.0731	2.0171	61.1
Column Cross section 10	5.2172	3.3379	3.4256	2.1865	58.1
Column Cross section 11	4.3794	2.5489	2.6209	1.7203	60.7
Row Cross section 1	6.9375	3.7005	3.6816	2.3578	66.0
Row Cross section 2	6.4972	2.9903	3.0293	1.7544	73.0
Row Cross section 3	4.5824	2.8843	2.9332	1.9631	57.2
Row Cross section 4	7.0182	3.4087	3.4013	2.0925	70.2
Row Cross section 5	6.5620	3.5779	3.5906	2.1577	67.1
Row Cross section 6	6.9686	3.3586	3.4280	2.2070	68.3
Row Cross section 7	6.8329	3.1977	3.2778	2.0975	69.3
Row Cross section 8	7.7733	3.7850	3.7997	2.1990	71.7
Row Cross section 9	5.7281	2.7969	2.9109	1.9301	66.3
Row Cross section 10	5.0358	2.3813	2.4803	1.5229	69.8
Row Cross section 11	2.3477	1.3837	1.4051	0.9383	60.0

Table 3 Root mean squared error for the results of smoothing and HNN downscaling algorithms with Nghe An 30 m DEM

Data sets	Original DEM (m)	Bilinear Smoothing (m)	Cubic Smoothing (m)	HNN downscaling (m)	Accuracy improvement (%)
Nghe An 30 m SRTM data	11.1379	8.8105	8.8736	8.3510	25.0
Column Cross section 1	8.5013	6.8408	6.9101	6.4673	23.9
Column Cross section 2	9.7106	8.4326	8.4863	8.5069	12.4
Column Cross section 3	11.6961	10.7635	10.8141	10.4270	10.9
Column Cross section 4	10.0198	8.9907	9.0225	8.3592	16.6
Column Cross section 5	9.2745	7.0420	7.2130	7.0696	23.8
Column Cross section 6	11.5945	9.8018	9.8618	9.7523	15.9
Column Cross section 7	9.7925	8.3543	8.4407	8.5220	13.0
Row Cross section 1	10.4429	9.8024	9.8357	9.3701	10.3
Row Cross section 2	9.9168	8.0953	8.0897	7.6225	23.1
Row Cross section 3	10.5144	9.6251	9.6645	9.3598	11.0
Row Cross section 4	9.9849	7.7341	7.8310	8.3409	16.5
Row Cross section 5	9.8911	8.4770	8.5192	7.6701	22.5
Row Cross section 6	8.8079	7.7367	7.7801	7.6159	13.5
Row Cross section 7	6.6352	6.4032	6.4005	6.3202	4.7

from bilinear and cubic smoothing is higher above and close with the original coarse resolution surface while the surface formed by the downscaled DEMs is lower and close to the 5 m reference surface. The HNN downscaling performed particularly better than the bilinear and cubic smoothing in the places like top of the ridges, hills or valley bottom, especially with the V-shape valleys and upside-down V-shape ridges and hills. This can be explained by the effects of the elevation constraint that help to reduce or increase the elevation at this points while the spatial dependence maximization function makes the elevations of the adjacent sub-pixels change gradually like in the real terrain.

Similar to the visual observation, the quantitative assessment based on RMSE in the Table 1, Table 2, Table 3 showed an improvement of HNN downscaling over the conventional smoothing methods. The RMSE decreased sharply for the HNN downscaling DEM to 0.8493 m from 2.4571 m, 1.5139 m, and 1.6000 m, for the original, bilinear and cubic smoothing, respectively, with the 5 m Lang son data. With the 20 m Nghe An data, the RMSE of the HNN downscaling DEM is 1.9853 m while the RMSEs of bilinear and cubic smoothing are 3.3716 m and 3.3716 m, respectively. Comparing with RMSE of the original 60 m data, the RMSE of downscaled 20 m reduced significantly by 72% from 6.9326 m to 1.9853 m. For the Nghe An 30 m test data, the improvement of HNN downscaling algorithm is not as sizable as for the 5 m and 20 m data sets but it is still very convincing with the RMSE reduced by 25% comparing with the original 90 m DEM. All of this statistics proved that the HNN downscaling will increase the accuracy of the gridded DEM at different resolutions. However, the algorithm seems to work better with the higher resolution DEMs.

The accuracy improvement based on RMSE values along the profiles demonstrates the effects of the terrain features to the algorithm. For the 20 m and 30 m data sets in Nghe An, the improvement of accuracy between the original and downscaled DEMs are relatively constant. For 30 m data set, accuracy improvement for most of profiles is between 10% and 20%. The range of accuracy improvement for 20 m data set is 20% between 50% and 70%. The accuracy improvement of 5 m data set is more various with the lowest value of 35% and the highest values of 49%. This can be explained by the fact that most part of profiles with good accuracy improvement of more than 65% such as column cross-sections number 2, 4 and row cross-sections number 2, 4, 9 located in the specific terrain such as valley bottom or top of the hill. Contrastively, the profiles with lower accuracy improvement crossed mostly in the sides of mountains where the surface of original DEM is relatively close to the reference DEM. The less variety of accuracy improvement of 20 m and 30 m data sets is because of the fact that most profiles of these data sets crossed along all different types of terrain rather than crossing mostly on specific terrain forms (Fig. 5).

4. Conclusions

In this paper, an algorithm for increasing the accuracy of gridded DEM is proposed and tested for different DEM resolution. The newly proposed downscaling algorithm is formulated using Hopfield neural network mechanism with a spatial dependence maximization goal function and a elevation constraint. The tests of newly proposed algorithm is implemented with three elevation data sets of 5 m gridded DEM in Lang Son province, 20 m and 30 m gridded DEMs in Nghe An province, Vietnam.

The testing results showed a sharp increasing in accuracy of the downscaled gridded DEMs in comparison with the original gridded DEM, bilinear and cubic smoothing. The visual assessment showed the higher similarity of the downscaled DEMs with the reference DEM image than the images of DEMs generated by bilinear and cubic smoothing. The analysis based on RMSE also showed the increasing in DEM accuracy and better results of the HNN downscaling algorithm over the results of bilinear and cubic smoothing. The RMSE of downscaled DEMs decreased by approximately 65%, 71% and 25% for 5 m DEM in Lang son province, 20 m and 30 m DEMs in Nghe An province. The RMSE values of downscaled DEM are lower in comparison with bilinear and cubic smoothing, especially for the 5 m and 20 m data sets.

The visual and quantitative assessment also showed that the HNN downscaling algorithm performed better for some specific terrain features such as valley bottom or crests of the ridges. The RMSE of the profiles located mostly in these terrain features decreased about 20% comparing with those of the profiles crossing mostly mountain sides or flat areas. This can be explained by the effects of the combination of elevation constraint and spatial dependence maximization function formulated by semivariance minimization.

Acknowledgements

This work was supported by Vietnam National Foundation of Science and Technology Development under the project 105.99-2014.15.

References

Atkins, Brian, Charles A Bouman, Jan P. Allebach, Jay S Gondek, Morgan T Schramm, and Frank W. Sliz. 2000. Computerized method for improving data resolution. US Patent US 6075926 A.

Atkinson, P. M. 1997. "Mapping sub-pixel boundaries from remotely sensed image." In *Innovation in GIS,* by Z Kemp. London: Taylor and Francis.

Bian, Ling, and Rachael Butler. 1999. "Comparing Effects of Aggregation Methods on Statistical and Spatial Properties of Simulated Spatial Data." *Photogrammetric Engineering & Remote Sensing* 65 (1): 73-84.

Chang, Kang-tsung, and Bor-wen Tsai. 1991. "The Effect of OEMResolution on Slope and Aspect Mapping." *Cartography and Geographic Information Systems* 69-77.

Guo, Qinghua, Wenkai Li, Hong Yu, and Otto Alvarez. 2010. "Effects of Topographic Variability and Lidar Sampling Density on Several DEM Interpolation Method." *Photogrammetric Engineering & Remote Sensing* 76 (6): 701-712.

Liu, Xiaoye. 2008. "Airborne LiDAR for DEM generation: some critical issues." *Progress in Physical Geography* 32 (1): 31-49.

Minh, Nguyen Quang. 2011. "Image smoothing of multispectral imagery based on HNN and Geostatistics." *China Journal of Remote Sensing* 640-644.

Nguyen, Q. M., P. M. Atkinson, and H. G Lewis. 2005. "Super-resolution mapping using Hopfield neural netwok with panchromatic image." Hanoi: Asian Conference on Remote Sensing ACRS, CD-ROM.

Rapinel, S., L. Hubert-Moy, B. Clément, Nabucet J., and C. Cudennec. 2015. "Ditch network extraction and hydrogeomorphological characterization using LiDAR-derived DTM in wetlands." *Hidrology Research* 46 (2): 276-290.

Rawat, Kishan Singh, Gopal Krishna, Amresh Mishra, Jitendra Singh, and Shashi Vind Mishra. 2014. "Effect of DEM data resolution on low relief region sub-watershed boundaries delineating using of SWAT model and DEM derived from CARTOSAT-1 (IRS-P5), SRTM and ASTER." *Journal of Applied and Natural Science* 144-151.

Saksena, Siddharth, and Venkatesh Merwade. 2015. "Incorporating the effect of DEM resolution and accuracy for improved flood inundation mapping." *Journal of Hydrology* 530: 180–194.

Schoorl, J. M., M. P. W. Sonneveld, and A. Veldkamp. 2000. "Three-dimensional land landscape process modelling: the effect of DEM resolution." *Earth Surface Processes and Landforms* 25: 1025-1034.

Smith, Michael P., A-Xing Zhub, James E. Burt, and Cynthia Stiles. 2006. "The effects of DEM resolution and neighborhood size on digital soil survey." *Geoderma* 137: 58-69.

Su, Y. F., G. M. Foody, A. M. Muad, and K. S. Cheng. 2012. "Combining Hopfield Neural Network and Contouring Methods to Enhance Super-Resolution Mapping." *IEEE Journal of Selected Topics in Applied Earth Observations and Remote Sensing* 5 (5): 1403 - 1417.

Tank, David W., and John J. Hopfield. 1986. "Simple " Neural" Optimization Networks: An A/D Converter, Signal Decision Circuit, and 'a Linear Programming Circuit." *IEEE Transactions on Circuits and Systems, VOL. CAS-33, NO. 5, MAY 1986* 33 (5): 533-541.

Tatem, A. J., H. G. Lewis, P. M. Atkinson, and M. S. Nixon. 2001. "Multi-class land cover mapping at the sub-pixel scale using a Hopfield neural network." *International Journal of Applied Earth Observation and Geoinformation* 3: 184-190.

Vieux, Baxter E. 1993. "DEM aggregation and smoothing effects on surface runoff modeling." *Journal of Computing in Civil Engineering* 7 (1): 310-338.